Dual-Isotope Brain SPECT Imaging with Technetium and Iodine-123: Validation by Phantom Studies

Michael D. Devous, Sr., James L. Lowe and J. Kelly Payne

Nuclear Medicine Center and Department of Radiology, The University of Texas Southwestern Medical Center, Dallas, Texas

Editor's Note: See also Dual-Isotope Brain SPECT Imaging with Technetium-99m and Iodine-123: Clinical Validation Using Xenon-133 SPECT on page 1919

Phantom studies were employed to determine whether the enhanced energy resolution (9.7% FWHM) of a new high-resolution, three-headed single-photon emission computed tomograph might permit the simultaneous acquisition of ^{99m}Tc and ^{123}I. Various window widths (15% and 10%) and positions (centered and asymmetric to the photopeak) were used to examine cross-contamination between these two isotopes. Brain phantom experiments using a 15% centered ^{99m}Tc window in conjunction with a 10% asymmetric ^{123}I window (upper half of the ^{123}I photopeak) demonstrated that approximately 95% of observed counts were derived from the isotope of interest. Shifting the ^{123}I window from asymmetric to centered resulted in a significant increase in contamination of the ^{123}I window. Shifting the ^{99m}Tc window from centered to asymmetric did not significantly alter image quality for ^{99m}Tc. Separate experiments employing vials with varying isotope concentrations demonstrated that quantitative recovery from mixed ^{99m}Tc and ^{123}I sources was equivalent to that from matched single-isotope sources ($r^2 \geq 0.90$).

J Nucl Med 1992; 33:2030–2035

The use of a single isotope for patient imaging in nuclear medicine can be complemented by studies employing two tracers to examine altered physiologic states in a common organ. The first dual-isotope studies, performed in the 1970s on patients with heart and lung disorders, involved sequential injections and acquisitions (*1*). While useful, sequential acquisitions are time-consuming and suffer from patient motion artifact between acquisitions. The advent of *simultaneous* imaging of two isotopes in different energy windows during a single acquisition eliminated this obstacle. Further, simultaneous dual-isotope acquisitions yield image pairs which are in perfect spatial registration to each other. Planar applications of the dual-isotope method have included the localization and determination of some types of parathyroid disease (*2,3*). Recently, dual-isotope procedures using single-photon emission computed tomography (SPECT) have been employed for cardiac infarct localization (*4*), prognosis following acute myocardial infarction (*5*) or inflammatory myocardial disease (*6*) and quantitative estimation of infarct size (*7*).

Simultaneous dual-isotope SPECT imaging of regional cerebral blood flow (rCBF) has been a desirable but elusive goal. Unlike the ^{201}Tl/^{111}In (*4,5*), ^{201}Tl/^{99m}Tc (*6,7*) or ^{201}Tl/^{123}I (*8*) labels used in other forms of dual-isotope SPECT imaging, the photopeaks of ^{99m}Tc and ^{123}I (140 and 160 keV, respectively), the primary isotopes used in brain imaging, are not adequately resolved by typical gamma cameras to separate the counts in one window from those in the other, preventing application of the dual-isotope method to the study of the brain.

Newer SPECT cameras have considerably improved energy resolution over their predecessors. We have conducted phantom experiments using a new triple-head camera to explore the potential for resolving ^{99m}Tc from ^{123}I with various energy-window widths and positions. Quantitative recovery of isotope counts was also examined during dual-isotope acquisitions relative to recovery using conventional techniques.

METHODS

Instrumentation

All studies were performed using a PRISM 3000-S triple-headed rotating gamma camera (Picker, Cleveland, Ohio). Energy resolution was 9.7% FWHM. High-resolution, parallel-beam collimators were used during collection of brain phantom studies, and the more recently available high-resolution fan-beam collimators were used during vial phantom experiments. Data were

Received Dec. 16, 1991; revision accepted Jul. 1, 1992.

For reprints contact: Dr. Michael D. Devous, Sr., Nuclear Medicine Center, UT Southwestern Medical Center, 5323 Harry Hines Blvd., Dallas, TX 75235-9061.

acquired in a 128 × 128 matrix by each head from 40 equally spaced stops at a radius of 13 cm over a 120° circular orbit yielding 360° acquisition with 120 projection images.

Brain Phantom Studies

A plastic brain phantom (Capintec, Inc., Ramsey, N.J.) was used to investigate cross-contamination from spatially segregated ^{99m}Tc and ^{123}I in simultaneous dual-window acquisitions. Twelve studies were conducted using different window combinations and isotopes present in the phantom according to the scheme presented in Table 1. Window placements in overlaid ^{99m}Tc and ^{123}I spectra from this tomograph are illustrated in Figure 1. Each scan was conducted for 5 min. The gray matter compartment of the phantom was filled with ^{99m}Tc (0.091 mCi/cc) and four acquisitions were performed according to the window settings in Table 1. Iodine-123 (0.023 mCi/cc) was placed in the white matter compartment and the four acquisitions were repeated with both isotopes present. The gray matter compartment was drained and washed to remove residual ^{99m}Tc and four final acquisitions were conducted with only ^{123}I present. The phantom was held in place by a rigid jig which was not moved between studies. The jig permitted exact relocation of the phantom.

Vial Phantom Studies

Quantitative recovery of isotope counts from mixed ^{99m}Tc and ^{123}I sources during dual-isotope acquisitions was compared to recovery from matched single-isotope sources. Gelled ^{99m}Tc, ^{123}I and ^{99m}Tc + ^{123}I sources were prepared in 20 cc glass vials (2 cm diameter) and placed within a water-filled phantom (16.5 cm diameter, 3300 cc volume). Window settings and isotope combinations are presented in Table 2. Ten ^{99m}Tc sources were prepared ranging from 170 to 650 μCi (Table 3). Similarly, ten ^{123}I sources ranged from 34 to 337 μCi. For the ten mixed sources, ^{99m}Tc ranged from 169 to 1062 μCi. However, a pipetting error during source preparation rendered two of these unusable. Iodine-123 in mixed sources ranged from 34 to 338 μCi, one of which was unusable due to a pipetting error.

Data Analysis

All images were reconstructed by backprojection using a ramp filter, attenuation corrected and treated with region of interest (ROI) analyses. Mean counts per pixel were obtained for each region for both windows. All counts were decay corrected to compensate for different acquisition start times.

Four regions were examined using the brain phantom: (1) cortical gray matter; (2) thalamus; (3) subcortical white; and (4) corpus callosum. Regions 1 and 2 were combined to represent gray matter and regions 3 and 4 were combined to represent white matter. Regions were identified from a two-dimensional representation of the middle portion of the phantom and were overlaid by computer in exactly the same location in each reconstructed image set. Brain images for each study were reconstructed into single slices 2.49 cm thick. Cross-contamination was measured by comparing count densities from these ROIs.

Images in vial phantom studies were reconstructed into single 5.62-cm thick slices. Circular 1.8-cm diameter vial ROIs were obtained for each vial for both windows. These regions included nearly the entire volume of the isotope(s) present.

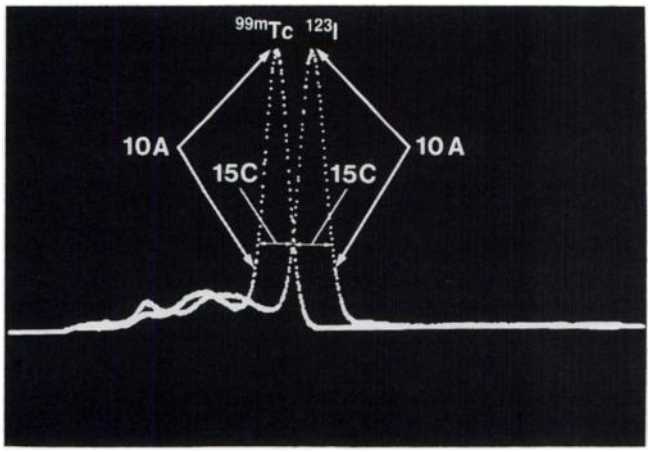

FIGURE 1. Window placements in overlaid ^{99m}Tc and ^{123}I energy spectra through one inch of Lucite scattering medium. 10A = 10% wide asymmetric window placement; 15C = 15% wide centered window placement.

RESULTS

Brain Phantom Studies

Images from typical brain phantom studies for ^{99m}Tc only, ^{123}I only ^{99m}Tc + ^{123}I are presented in Figures 2, 3

TABLE 1
Window and Isotope Combinations for Brain Phantom Studies

Isotope present	Tc window*	I window*
^{99m}Tc	10% Asymmetric	10% Asymmetric
^{99m}Tc	15% Centered	10% Asymmetric
^{99m}Tc	10% Asymmetric	15% Centered
^{99m}Tc	15% Centered	15% Centered
^{99m}Tc + ^{123}I	10% Asymmetric	10% Asymmetric
^{99m}Tc + ^{123}I	15% Centered	10% Asymmetric
^{99m}Tc + ^{123}I	10% Asymmetric	15% Centered
^{99m}Tc + ^{123}I	15% Centered	15% Centered
^{123}I	10% Asymmetric	10% Asymmetric
^{123}I	15% Centered	10% Asymmetric
^{123}I	10% Asymmetric	15% Centered
^{123}I	15% Centered	15% Centered

* Asymmetric: ^{99m}Tc = 10% ending at center of photopeak and ^{123}I = 10% starting at center of photopeak.

TABLE 2
Window and Isotope Combinations for Vial Phantom Studies

Isotope present	Tc window*	I window*
^{99m}Tc	10% Asymmetric	10% Asymmetric
^{99m}Tc	10% Centered	10% Centered
^{99m}Tc	15% Centered	10% Asymmetric
^{99m}Tc + ^{123}I	10% Asymmetric	10% Asymmetric
^{99m}Tc + ^{123}I	10% Centered	10% Centered
^{99m}Tc + ^{123}I	15% Centered	10% Asymmetric
^{123}I	10% Asymmetric	10% Asymmetric
^{123}I	10% Centered	10% Centered
^{123}I	15% Centered	10% Asymmetric

* Asymmetric: ^{99m}Tc = 10% ending at center of photopeak and ^{123}I = 10% starting at center of photopeak.

TABLE 3
Tube Activity (μCi) for Vial Phantom Study

Vial	Single-Isotope vials		Mixed-Isotope vials*		
	^{99m}Tc	^{123}I	^{99m}Tc	^{123}I	Tc/I
1	170	34	169	34	5.0
2	212	55	NU	74	—
3	224	97	223	NU	—
4	273	109	293	338	0.9
5	294	337	361	94	3.8
6	325	174	NU	206	—
7	362	94	477	136	3.5
8	429	113	496	186	2.7
9	498	186	730	144	5.1
10	650	224	1062	275	3.9

* NU = not used due to pipetting error.

and 4, respectively. For display purposes only, images from a window over an isotope not actually present in the phantom (e.g., ^{123}I in ^{99m}Tc only studies) were scaled to match the pixel brightness in the images from the "hot" window.

When only ^{99m}Tc was present, the ^{123}I images (Fig. 2) were structured similarly to the ^{99m}Tc images regardless of the window setting, although there were too few counts in the 10% asymmetric (10A) ^{123}I window to reconstruct a coherent image and low-count induced reconstruction artifacts are visible in the remaining I-window images. This structure suggests that the up-contamination of the ^{123}I window by ^{99m}Tc consisted primarily of photopeak events. When the ^{123}I window was 10A, contamination was 1.0% ± 0.8% of the counts in the 15% centered (15C) ^{99m}Tc window. When the ^{123}I window was 15C, up-contamination from ^{99m}Tc was 5.4% ± 0.3%.

When only ^{123}I was present, the images from the ^{99m}Tc window evidenced reduced structure relative to the ^{123}I images regardless of the ^{99m}Tc window setting (Fig. 3). This suggests that the down-contamination of the ^{99m}Tc window by ^{123}I consisted primarily of Compton scatter. When the ^{99m}Tc window was 15C, down-contamination was 22% ± 5% of the counts in the 15C ^{123}I window. When the ^{99m}Tc window was 10A, contamination was 11% ± 4%. No significant change in image quality was observed across window settings, demonstrating the relative insensitivity for ^{99m}Tc to window width and placement. For both ^{99m}Tc and ^{123}I, cross-contamination was consistent regardless of the location of the ROI (i.e., not spatially dependent).

When both isotopes were present, a 4:1 ratio for ^{99m}Tc to ^{123}I was used, similar to that expected for a clinical administration of 3 mCi IMP and 20 mCi HMPAO, taking into account the higher extraction fraction of IMP. Under such conditions, 94.5% ± 1% of the counts in a 15C ^{99m}Tc

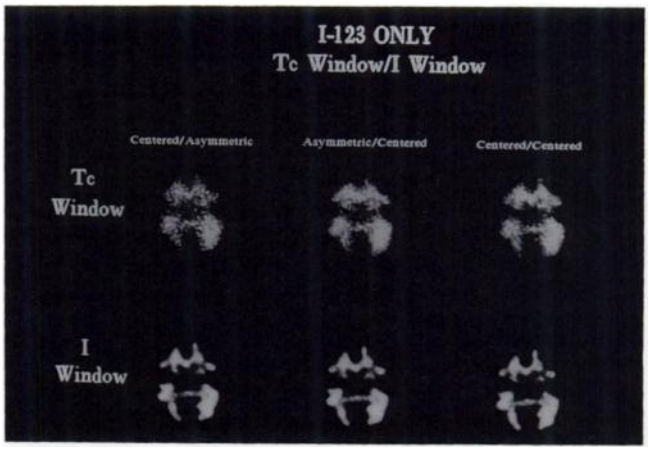

FIGURE 3. Dual-isotope images obtained from the brain phantom with only ^{123}I present in the white matter compartment. Window settings are as in Figure 2. Technetium-99m images were up-scaled to match maximum pixel brightness in the ^{123}I window.

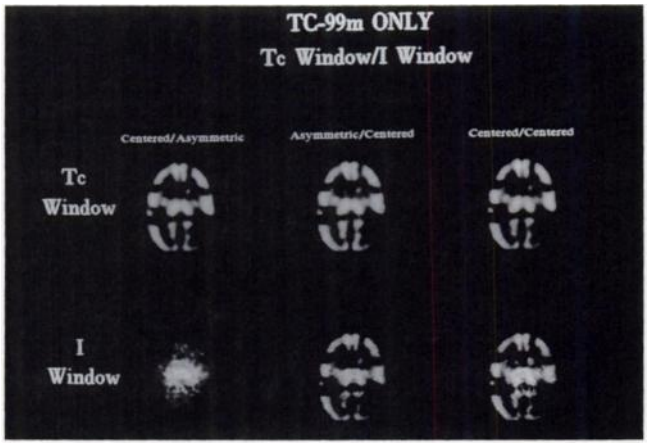

FIGURE 2. Dual-isotope images obtained from the brain phantom with only ^{99m}Tc present in the gray matter compartment. Asymmetric windows are 10% wide; centered windows are 15% wide. Iodine-123 images were up-scaled to match maximum pixel brightness in the ^{99m}Tc window.

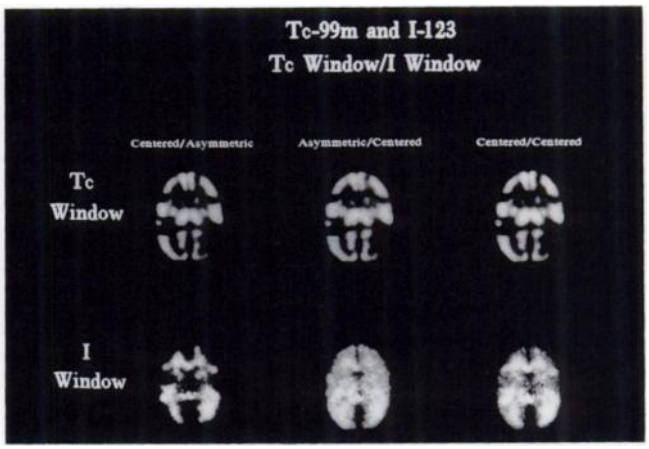

FIGURE 4. Dual-isotope images from the brain phantom with ^{99m}Tc in the gray matter compartment and ^{123}I in the white matter compartment in a relative ^{99m}Tc/^{123}I concentration ratio of 4:1. Images are all scaled to equal maximum pixel brightness.

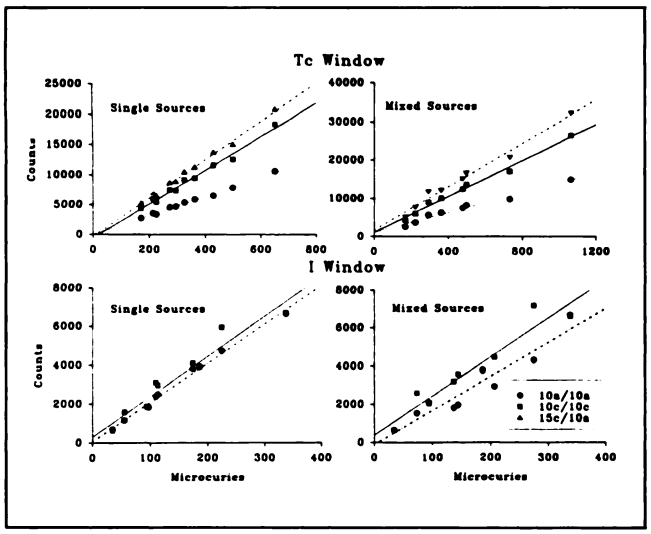

FIGURE 5. Correlations between observed count densities and vial μCi for studies in which vials contained only ^{99m}Tc, only ^{123}I, or mixed ^{99m}Tc and ^{123}I sources. Correlation coefficients, slopes and intercepts are listed in Table 5. 10A = 10% wide asymmetric window placement; 10C = 10% wide centered window placement; 15C = 15% centered window placement.

window would be expected to be from ^{99m}Tc and 96.0% ± 3% of the counts in a 10A ^{123}I window would be expected to be from ^{123}I (left column, Fig. 4). Switching from 15% centered ^{99m}Tc/10% asymmetric ^{123}I (15C/10A) to 10A/15C or 15C/15C had no effect on ^{99m}Tc images (center and right columns, Fig. 4). However, ^{123}I images were severely degraded by up-contamination from ^{99m}Tc in either of the latter window configurations.

Vial Studies

Correlation between observed count densities and vial tube activity are shown for ^{99m}Tc only, ^{123}I only and ^{99m}Tc + ^{123}I for both windows in Figure 5. Regression results for observed counts versus true activity are presented in Table 4. Regression results for relative activity ratios are presented in Table 5.

When ^{99m}Tc only was present, using a 15C window, a linear relationship (r^2 = 0.99) was observed between recovered counts and tube activity. When a 10C window was used, the relationship was still linear (r^2 = 0.99) and there was a small but statistically significant decrease in slope. For both 15C and 10C windows, intercepts were not significantly different from zero. When the ^{99m}Tc window was 10A, as expected, slope decreased significantly but the relationship remained linear (r^2 = 0.99). Intercept did not differ from zero or from those for 15C and 10C windows. In mixed-source acquisitions, ^{99m}Tc correlations and slopes were similar to those obtained from single-source studies. However, intercepts were higher for all ^{99m}Tc windows reflecting an increase in counts from ^{123}I Compton scatter.

When ^{123}I only was present, linear relationships were also observed when the ^{123}I window was 10A. Two separate 10A windows were collected, one against a 10A ^{99m}Tc window and the other against a 15C ^{99m}Tc window. Data points and regression lines from these windows were virtually indistinguishable from one another (Table 4). When the ^{123}I window was 10C, the relationship remained linear and the slope was unchanged. A small upward shift in intercept occurred from increased counts, although the intercept was still not significantly different from zero. Mixed-source ^{123}I data, while showing greater variability than that observed in single-isotope acquisitions, retained the same relationships and strong correlations ($r^2 \geq 0.90$).

We also examined the relationship between ratios within recovered counts to ratios within tube activity in order to determine if *relative* distributions of counts within a sample were affected by dual-isotope acquisitions. For ratio data, significant linear regressions were obtained for all comparisons (Table 5). Slopes were generally not significantly different from one (indicating correct recovery of true dose distributions) and were not significantly altered by the mixed-source environment. Intercepts were less accurately determined in the mixed source data, but were still not significantly different from zero.

TABLE 4
Count Versus μCi Regressions for Vial Phantom Studies*

		Single Sources		Mixed Sources	
		^{99m}Tc	^{123}I	^{99m}Tc	^{123}I
10% A/10% A	r^2	0.99	0.99	0.98	0.91
	m	16 ± 0.5	20 ± 0.6	13 ± 0.8	18 ± 2
	b	24 ± 167	98 ± 105	1176 ± 458	−89 ± 409
10% C/10% C	r^2	0.99	0.93	0.99	0.92
	m	28 ± 1	21 ± 2	24 ± 1	20 ± 2
	b	−486 ± 446	320 ± 333	1176 ± 600	398 ± 440
15% C/10% A	r^2	0.99	0.99	0.98	0.91
	m	32 ± 0.9	20 ± 0.5	28 ± 2	18 ± 2
	b	−255 ± 330	71 ± 89	1774 ± 867	102 ± 413

* m (slope) and b (intercept) ± s.e.

TABLE 5
Ratio Regressions for Vial Phantom Studies*

		Single Studies		Mixed Studies	
		^{99m}Tc	^{123}I	^{99m}Tc	^{123}I
10% A/10% A	r^2	0.99	0.99	0.98	0.91
	m	0.99 ± 0.03	1.00 ± 0.03	0.85 ± 0.05	0.95 ± 0.11
	b	0.01 ± 0.06	0.14 ± 0.15	0.16 ± 0.18	−0.14 ± 0.63
10% C/10% C	r^2	0.99	0.93	0.99	0.92
	m	1.09 ± 0.05	1.11 ± 0.11	0.93 ± 0.04	1.09 ± 0.12
	b	−0.11 ± 0.10	0.50 ± 0.52	0.28 ± 0.14	0.61 ± 0.68
15% C/10% A	r^2	0.99	0.99	0.98	0.90
	m	1.04 ± 0.03	1.03 ± 0.03	0.92 ± 0.05	0.93 ± 0.11
	b	−0.05 ± 0.06	0.11 ± 0.13	0.34 ± 0.17	−0.16 ± 0.63

* m (slope) and b (intercept) ± s.e.

Source concentrations were arranged to compare the effects of a range of "contaminant" activity on primary source activity between single-source data (no contaminant) and mixed-source data (compare single-source/mixed-source ^{99m}Tc vial pairs 1/1, 3/3, 5/4, 7/5, 9/8 and ^{123}I pairs 1/1, 3/5, 5/4, 7/5 and 9/8). The data presented in Figure 5 support the conclusion that quantitative count recovery is not a function of the concentration of "contaminant" over the range of activities examined (Table 3).

DISCUSSION

Simultaneous dual-isotope imaging of the brain phantom separated isotope distributions for a 15% centered ^{99m}Tc window when combined with a 10% asymmetric ^{123}I window. No significant differences in image quality were observed between the 15C and the 10A ^{99m}Tc window. Although the contamination from ^{123}I was twice as high in a 15C window as in a 10A window, in the typical ^{99m}Tc/^{123}I dose relationship expected for clinical studies, net contamination is only changed from 5% for a 15C window to 3% for a 10A window. The increased count rate obtained in the 15C window likely offsets this small increase in contamination. Thus, ^{123}I contamination of the ^{99m}Tc window was relatively independent of position or width (taking into account width-based count differences).

In contrast, a marked increase in contamination was observed when the ^{123}I window was shifted from 10A to 15C. The five-fold increase in contamination in a 15C window relative to a 10A window is amplified by the typical four-fold greater ^{99m}Tc activity relative to ^{123}I activity used in clinical settings. Thus, ^{99m}Tc contamination of the ^{123}I window was sensitive to both width and position.

In vial experiments, isotope concentrations were recovered as accurately from asymmetric dual-isotope SPECT as from conventional windows. Both absolute counts and count ratios were linearly related ($r^2 >= 0.90$) between single- and dual-isotope studies under all examined conditions. These data lend quantitative support to the image data obtained with the brain phantom. Replication of single-isotope count recovery by the dual-isotope technique affirms the accuracy of dual-isotope imaging as a quantitative tool.

The brain phantom experiments were used to determine the degree of cross-contamination from spatially discrete sources of ^{99m}Tc and ^{123}I. These data suggest that contamination of ^{99m}Tc by the Compton downscatter of ^{123}I is low when the ^{99m}Tc:^{123}I ratio is 4:1. Even at a 1:1 ratio, such as seen in Figure 1, the cross-talk is small. Up-contamination of ^{123}I by ^{99m}Tc photopeak events is small only when an asymmetrically high energy window is used for ^{123}I. Since spatially discrete sources (brain phantom experiments) cannot judge the effect of a contaminant source on count recovery of the principal source, we used vials of co-mingled ^{99m}Tc and ^{123}I over a range of activities and relative ratios. The vial experiments demonstrated that linear count recovery of ^{99m}Tc was unaffected in slope by the presence of ^{123}I, but an increase in intercept was observed due to the scatter contribution. Iodine-123 count recovery was unaffected either in slope or intercept by the presence of ^{99m}Tc when a 10% wide, high asymmetric window was employed.

The ability to perform single acquisition dual-isotope scans in the brain provides a powerful clinical tool. Also, the simultaneous collection of two image sets positionally linked together facilitates mathematical operations between data sets, such as image subtraction. This particular clinical application has been explored and validated. The results appear in a companion manuscript (*9*).

ACKNOWLEDGMENTS

The authors would like to express gratitude to S.K. Gassaway for expert technical assistance.

REFERENCES

1. Fujii T, Kanai H, Mirayama J, et al. Myocardial imaging with thallium-201—subtraction imaging with ^{201}TlCl and ^{99m}TcO$^{-}_{4}$ for the visualization of the right ventricle. *Radioisotopes* 1979;28:751–756.

2. Ziffer JA, Fajman WA. Ectopic parathyroid gland localization with thallium-201 SPECT. *Clin Nucl Med* 1987;12:617–619.
3. Winzelberg GG, Hydovitz JD, O'Hara KR, et al. Parathyroid adenomas evaluated by Tl-201/Tc-99m pertechnetate subtraction scintigraphy and high resolution ultrasonography. *Radiology* 1985;155:231–235.
4. Johnson LL, Seldin DW. The role of antimyosin antibodies in acute myocardial infarction. *Semin Nucl Med* 1989;19:238–246.
5. Johnson LL, Seldin DW, Keller AM, et al. Dual isotope thallium and indium antimyosin SPECT imaging to identify acute infarct patients at further ischemic risk. *Circulation* 1990;81:37–45.
6. Kitahara K, Suzuki S, Takayama Y, Hiroe M. New color imaging of [^{99m}Tc]pyrophosphate and [^{201}Tl]chloride dual isotope single photon emission computed tomography in acute myocarditis. *Jpn J Nucl Med* 1989;26:773–779.
7. Kawaguchi K, Sone T, Tsuboi H, et al. Quantitative estimation of infarct size by simultaneous dual radionuclide single photon emission computed tomography: comparison with peak serum creatine kinase activity. *Am Heart J* 1991;121:1353–1360.
8. Nishimura T, Uehara T, Oka H, et al. Serial assessment of denervated but viable myocardium following acute myocardial infarction by using ^{123}I-MIBG and ^{201}TlCl myocardial SPECT. *Jpn J Nucl Med* 1990;27:709–718.
9. Devous MD Sr, Payne JK, Lowe JL. Dual-isotope brain SPECT imaging with ^{99m}Tc and ^{123}I. Clinical validation using ^{133}Xe SPECT. *J Nucl Med* 1992;33:000–000.

(continued from page 1993)

SELF-STUDY TEST
Skeletal Nuclear Medicine
ANSWERS

technetium, some of which will then be in the +7 valence state as ^{99m}Tc pertechnetate. Hence, the saline used to reconstitute preparations of ^{99m}Tc MDP should be highly deoxygenated and preservative free.

Gentisic acid is an anti-oxidant, as is ascorbic acid. Both agents protect the stannous ion and technetium from oxidation by oxygen or radiolytic products. The pattern shown in Figure 1 is not typical of excessive free ^{99m}Tc pertechnetate, in which excessive gastric activity would be expected (Fig. II).

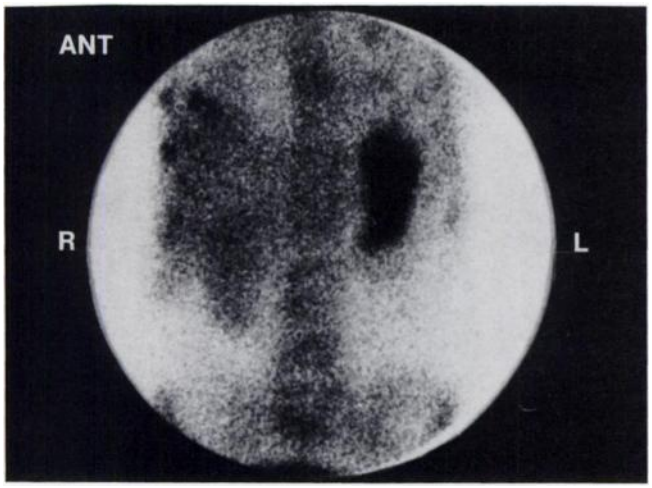

References
1. Owunwanne A, Church LB, Balu M. Effect of oxygen on the reduction of pertechnetate by stannous ion. *J Nucl Med* 1977;18:822–826.
2. Ponto JA, Swanson DP, Freitas JE. Clinical manifestations of radiopharmaceutical formulation problems. In: Hladik WB III, Saha GB, Study KT, eds. *Essentials of Nuclear Medicine Science*. Baltimore: Williams & Wilkins, 1987:268–289.
3. Tofe AJ, Bevan JA, Fawzi MB, Whitehouse HS, Francis MD. Antioxidant stabilization of bone agents. In: Sodd VJ, Allen DR, Hoogland DR, Ice RD, eds. *Radiopharmaceuticals II*. New York: Society of Nuclear Medicine, 1979:637–644.

ITEMS 6–10: Diffuse Renal Parenchymal Localization of ^{99m}Tc MDP

ANSWERS: 6, T; 7, T; 8, F; 9, F; 10, T

The scintigrams shown in Figure 2 demonstrate diffusely increased activity in thoracic and lumbar vertebrae and in both iliac bones. There also are focal lesions in the left lesser trochanter, several ribs, and the calvarium. (The large right parietal "doughnut" lesion actually was due to a prior craniotomy for resection of a solitary cerebral metastasis.) These osseous abnormalities most likely reflect widespread metastatic disease.

In addition, there is intensely increased activity in the parenchyma of both kidneys. In this clinical setting, the most likely explanation for this finding is hypercalcemia associated with multiple skeletal metastases. Less often, in a patient with cancer of the lung, the hypercalcemia would be due to a humoral mechanism. Recent anticancer chemotherapy with a variety of drugs, including cyclophosphamide, vincristine, and doxorubicin, also has been observed to cause similar scintigraphic findings. Additionally, intense renal parenchymal localization of ^{99m}Tc diphosphonates may be seen in patients with iron overload due to multiple transfusions or hemochromatosis.

With early obstructive uropathy, the retained renal activity may appear to be predominantly parenchymal in location. Much more often with obstruction, the tracer can be seen to be clearly within the dilated collecting system and ureter. In this patient, the absence of columning of activity in the ureters, the "normal" size of the bladder (arguing against bladder outlet obstruction), and the parenchymal rather than pelvicalyceal distribution of the renal activity all make bilateral obstructive uropathy an unlikely explanation for the scintigraphic findings.

Although cancer of the lung commonly metastasizes to the kidneys (twice as common at autopsy as renal cell carcinoma), renal metastases would not cause diffusely increased parenchymal uptake of ^{99m}Tc MDP. Rather, focal deposits would appear as localized areas of decreased activity and diffuse infiltration might lead to a generalized decrease in activity in an enlarged kidney.

References
1. Burtis WJ, Wu TL, Insogna KL, Stewart AF. Humoral hypercalcemia of malignancy. *Ann Intern Med* 1988;108:454–457.
2. Buxton-Thomas MS, Wraight EP. High renal activity on bone scintigrams. A sign of hypercalcemia. *Br J Radiol* 1983;56:911–914
3. Choy D, Murray IPC, Hoschl R. The effect of iron on the biodistribution of bone scanning agents in humans. *Radiology* 1981;140:197–202.
4. Lutrin CL, McDougall IR, Goris ML. Intense concentration of technetium-99m pyrophosphate in the kidneys of children treated with chemotherapeutic drugs for malignant disease. *Radiology* 1978;128:165–167.

ITEMS 11–16: Photon-Deficient Femoral Capital Epiphysis

ANSWERS: 11, T; 12, T; 13, T; 14, T; 15, T; 16, F

The pinhole images in Figure 3 show absence of tracer uptake in the left femoral capital epiphysis, indicating a compromised blood supply. The childhood disorder most commonly associated with this scintigraphic finding is Legg–Perthes disease, an idiopathic form of avascular necrosis. Any infiltrative disease, such as Gaucher's disease and osteomyelitis, may compromise the blood supply to the femoral capital epiphysis as the infiltrative process (engorged macrophages, pus, tumor) expands within the bone marrow cavity. When this occurs, the bone-seeking radiopharmaceutical is not delivered to the site of disease, and a photopenic area will result.

The fluid within the capsule of the hip in association with hemarthrosis, septic arthritis, and transient synovitis may raise the pressure within the joint to such an extent that it impairs blood flow to the femoral capital epiphysis, causing a "cold" region scintigraphically. If the fluid is removed promptly, the activity generally will return on a subsequent study, but if the increased pressure is sustained for a prolonged time, osteonecrosis may result. This is most likely to occur with septic arthritis, in which drainage of the hip joint should be performed as a surgical emergency.

Chondroblastoma is an uncommon primary bone tumor most often

(continued on page 2044)